Optical space telescope without mirrors

Thomas D. Ditto*[ab], Mei-Li Hsieh[b] , Heidi Jo Newberg[b] , Leaf Swordy[b]
Robert Hoyt[c], Jesse Cushing[c]
[a] 3DeWitt LLC, P.O. Box 83, Ancramdale, NY 12503-0010;
[b] Dept. of Physics, Applied Physics & Astronomy, Rensselaer Polytechnic Institute, Troy, NY
[c] Tethers Unlimited Inc, 11711 North Creek Pkwy # D113, Bothell, WA 98011-8808, USA

ABSTRACT

A notional space telescope without any mirrors or lenses is being investigated. DUET (Dual Use Exoplanet Telescope) has a gossamer membrane annular Gabor Zone Plate primary objective that is flat. Highly chromatic stellar imagery is disambiguated in a secondary also made from diffractive elements. The data acquired is intrinsically spectrographic and could (1) detect radial velocity below 5 cm/sec and (2) take direct spectra of a systems exoplanets. DUET is intended as a follow-up to a survey telescope, THE MOST, being developed in tandem which will identify target stellar systems with earth-like exoplanets. DUET observes one star at a time, integrating its light until the exoplanetary system is resolved. DUET utilizes a battery of coronographic methods including angular differential imaging, interferometric nulling, and phased Fraunhofer line subtraction. The potential performance has been given preliminary laboratory tests which are detailed in Conference AS11451-192.

Keywords: exoplanet, spectroscopy, holography, Gabor Zone Plate, Newton Prism Experiment, Dittoscope

1. INTRODUCTION

The default selections for the primary objectives and secondaries of contemporary astronomical telescopes are mirrors. Ancillary optics are generally either reflective or refractive elements. Dispersive elements are typically reserved for spectrographs in the optical train. In proposed space telescopes, primary mirrors impose mass and diameter limitations. Incremental engineering developments have improved performance, [1] but primary objective mirrors deployed in space are invariably of smaller diameters than the largest ground-based mirrors. Space telescope mirror primaries are typically manufactured on the ground and must be stowed in a manner to withstand the rigors of their launch.

Newton's Dual Prism Experiment has never been the premise of a telescope prior to ours in the twenty first century. Indeed, in the seventeenth century, endemic chromatic aberration of refractors led to the preferred achromatic behavior exhibited by reflectors. Yet one cannot help notice that the spectrum of the sun formed by Newton's dual prism apparatus is a spatial magnification color by color of white light striking prisms. The utility of this spread had no known practical application in Newton's time, but by the nineteenth century the "bar code" represented by stellar spectra was better appreciated. The focused image of a star at the image plane has no areal dimension to speak of, but its spectrum can be spread out to a considerable length revealing details about the composition, the age, and the motion of a star.

As Newton reported in *Opticks* the rotation of his primary prism caused a rotation of the position and change in the color of the light passing through the secondary prism.[2] If this phenomenon was implemented to observe every star in the sky, each one would appear at a different position and in a different color as viewed after the second prism.

1.1 Diffractive primary objective telescopy

At the 2002 SPIE Astronomical Telescope and Instrumentation Conference, the notion of a primary objective grating telescope, eponymously named the Dittoscope, was disclosed for the first time. [3] No prior art was found in the literature by attendees or in the years to follow. The novel concept was that a plane grating primary objective collects starlight in its first diffraction order and a secondary parabolic mirror focuses wavefronts collected from the primary at a fixed angle of diffraction. To disambiguate the overlapping wavelengths, the light is focused by the secondary parabolic mirror to be processed by an adjustable notch filter. At the resulting image plane, a source would be detected at a unique wavelength at a unique incident angle. In effect, a spectrum was projected onto the sky. One embodiment presumed ground deployment where the Earth was a drift scan platform by virtue of its rotation. The spectrum for any object was collected as a series of frames much like a motion picture. One embodiment aimed at ground deployment.[4] A 2002 paper on space deployment was not included in its conference *Proceedings*, but was published later at Photonics North in 2004.[5]

*td@3dewitt.com http://www.3dewitt.com

1.2 Parameterization of the original Dittoscope concept

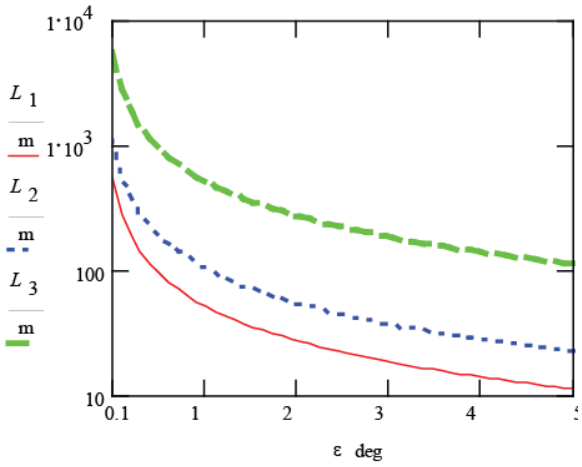

Fig. 1 Length L in meters vs grazing angle ε in degrees for secondary mirror diameters of **1**, **2** and **10** meters.

The secondary parabolic mirror used in the Dittoscope forms a kind of "fulcrum" upon which the telescope gains in "leverage" or magnification M that depends on the length L of the grating. $M \approx L/\Delta\lambda$, where $\Delta\lambda$ is the wavelength resolution. Angle r is the receiving angle of reconstruction subtended from the surface normal of the grating. As the angle ε of grazing exodus ($\varepsilon = 90° - r$) decreases, the length L can increase exponentially, Figure 1.This relationship has the potential for extremely long apertures in the dimension along which the secondary mirror captures diffracted light.

There are interdependent parameters idiosyncratic to this telescope. Integration time for any narrow wavelength band $\Delta\lambda$ captured within a frame time Δt is controlled by a combination of the diameter D of the secondary parabolic mirror, the angle of grazing exodus, ε, as well as the angle of rotation of the primary relative to lines of longitude and latitude, and the rate of the rotation of the Earth. The reader is referred to discussions in SPIE conference papers and NASA *Reports* for derivations.[6] A discussion of Δt for ground-based operations first appeared in 2004 [7] and is presented at this conference in paper 11445-293, a Dittoscope called TWO or Trip Wire Optics for near earth object surveillance.

2. WAVE GUIDE PRIMARY OBJECTIVE

Parameterization relevant to the present discussion are: 1) throughput efficiency η and 2) selection of a primary objective optic that has power to focus diffracted light without use of a secondary parabolic mirror.

2.1 Primary objective grating efficiency

As shown, L is maximized as the grazing angle ε decreases grating length, Figure 1, but efficiency η decreases, Figure 2.

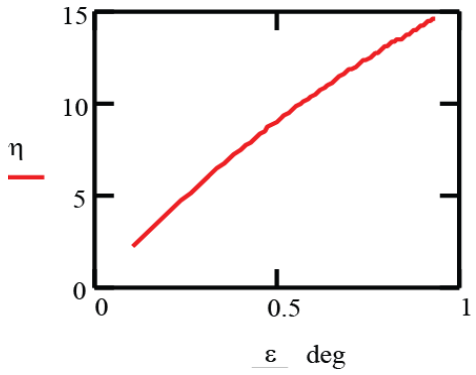

Fig. 2 Efficiency vs. angle of grazing exodus

In the case of the surface relief type of grating exampled by mechanically ruled types, adjacent grooves trap and scatter increasing percentages of the light reradiated from the primary grating surface as $\varepsilon \rightarrow 0°$. A vignette effect between the adjacent grooves makes an increase in grating length a zero-sum game, because while more collector is presented to the incoming starlight by virtue of lower grazing angle, scattered photons emitted between the grooves are lost. This phenomenon at low angles of ε is further compounded when metal coated reflection gratings are used. Induction caused when the transverse electrical wave is proximate to a metalized surface produces a current that attenuates reradiated flux for that transverse wave polarization. Not only that, reflection gratings carry the penalty that the figure error in the non-diffracted dimension must conform to the sub-wavelength figure tolerances required of mirrors.

Transmission surface relief gratings enjoy immunity from electrical induction caused by metalized surfaces and have a significant additional advantage over reflection gratings in their relaxed surface figure error tolerances. However, efficiency suffers at low angles of ε when surfaces are uneven. Again, the redirected wavefronts from the grooves can be blocked by adjacent grooves that are in the path of diffracted wavefronts. The problem comes to bear where $\varepsilon < 1°$. This is the region where grating length grows exponentially, as illustrated in Figure 1. As L increases, grating efficiency η decreases pretty much in lock step, making photon collection at the secondary a zero sum game. The outcome is that at $\varepsilon = 0°$ where the grating length is unbounded, no light can find its way to the secondary optics, because $\eta = 0$. It is true that at this boundary the primary aperture is the greatest, but the resulting magnification is obviously useless if no photons are collected.

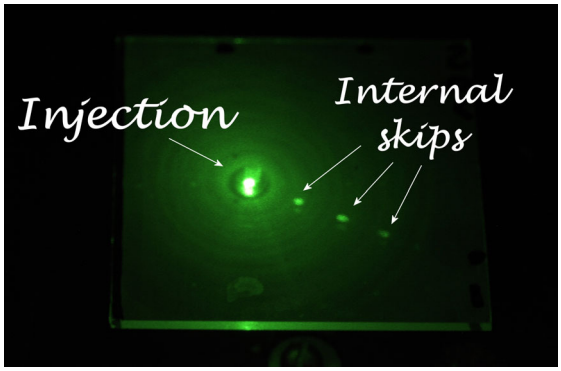

Fig. 3 Laser beam trapped in glass below critical angle

There are no surface relief profiles in phase gratings. For example, in holographic emulsions that periodically vary index of refraction to cause diffraction, light is not trapped in valleys and scattered. However, it turns out that at angles of grazing exodus, the grating to air interface causes light to be reflected back into both the holographic emulsion and its substrate as dispersion approaches the critical angle, Figure 3. As the length L grows, diffraction efficiency η decreases.

That said, when trapped by the critical angle, light can be collected at the distal end of the substrate that supports a grating if the substrate is configured as a wave guide. We have shown that light trapped in the substrate by total internal reflection (TIR) is available to be collected, Figure 4. This approach can eliminate the secondary mirror of a Dittoscope if, for example, the substrate can focus the trapped wavefront onto a sensor. Such a concept accompanied the earliest disclosure of the Dittoscope [8] reproduced here below as Figure 5.

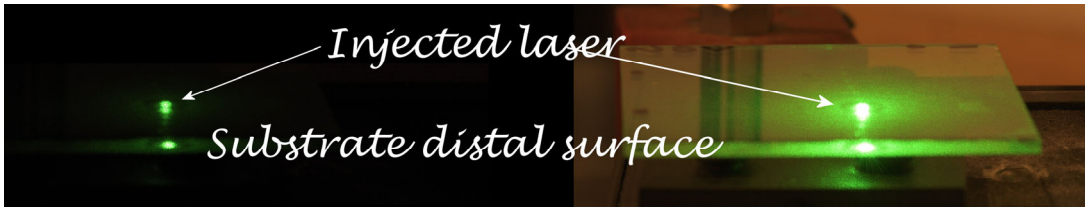

Fig.4 Total internal reflected (TIR) image of point source laser beam diffracted by holographic phase plane grating

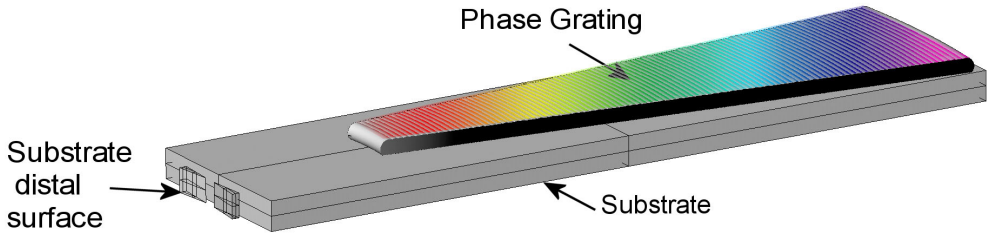

Fig. 5 CAD rendering of a curved rule phase grating combined with a substrate that relays a diffraction image by TIR

A prediction of a possible improvement in efficiency that might occur when the grazing exodus angle goes to 0° and the flux is tunneled to the distal surface by TIR is graphed in Figure 6. The predicted improvement has been spliced to the lowest values found in the graph of Figure 2 and is justified heuristically by the experiment of Figure 4.

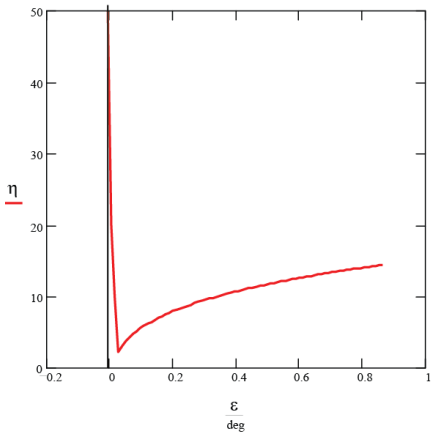

Fig. 6 Predicted efficiency at grazing exodus of a wave guide primary objective

2.2 Chirped holographic primary objective with curved fringes

The question remains how an image can be formed at the substrate distal surface by an unfocused wavefront diffracted by a surface phase grating. Experiments with gratings formed with curved rules suggest that when the fringes of the phase grating are in the form of arcs, the diffracted light originating as a plane wave are focused by optical physics similar to a Gabor Zone Plate (GZP). The phase grating could be a segment of a GZP which has the power to focus light trapped by TIR onto a spectrographic secondary according to the dual dispersion paradigm. With this in mind, we postulate a GZP primary objective grating telescope.

3. GABOR ZONE PLATE

We propose using a Gabor Zone Plate (GZP) as the primary objective of a space telescope, shown diagrammatically in Figure 7. Like the Fresnel lens from the nineteenth century, the twentieth century optical element named after Dennis Gabor has the power to focus. The rings in a GZP are similar to a Fresnel lens in that their periods vary inversely in proportion to their diameter. However, GZP ring periodicity is in the regime of the wavelengths they focus and exhibit far greater chromatic aberration than Fresnel lenses. Unlike a Fresnel lens, GZP focal length is inversely proportional to incident wavelengths. In a dual dispersion architecture, this seeming chromatic "bug" is a needed feature, because a secondary disperser is used to convert chromatic "error" into angular data. Like a Fresnel lens, the GZP form factor is flat. Indeed, a GZP is flatter than a Fresnel lens, because a GZP has no refractive lens rings. A GZP can be fabricated on a gossamer membrane at a low areal mass, recommending it for space deployment.

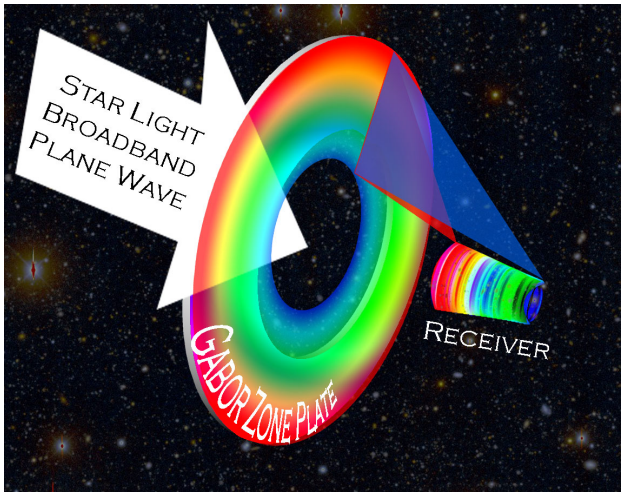

Fig. 7 Plane waves from stars are collected by a GZP and focused by wavelength onto a secondary spectrometer

In practice, a GZP can be no thicker than the substrate upon which the diffractive element rests. Contrast this with a MODE lens which combines a Fresnel and a GZP to control chromatic aberration but is not a flat membrane and exhibits limited bandwidth at its diffraction limit. [9] The Fresnel Zone Plate (FZP) has been investigated as a primary objective for astronomical telescopes. Like a GZP the FZP is no thicker than the substrate upon which it rests. FZP's also share the chromatic aberration issues associated with GZP's. Prior art in both FZP [10] and related photon sieve primaries [11] would have been suitable for the dual dispersion design but were preliminarily investigated without the critical dispersive secondary we specify to overcome chromatic aberration. While FZP and photon sieves could have been configured in double dispersers, we select GZP's in preference to FZP's, because we believe GZP's enjoy the potential for higher efficiency, due to fringe by fringe variation in blaze or refractive index that can to modified to optimize throughput.

3.1 GZP efficiency

A GZP would suffer from a similar loss of efficiency as plotted in Figure 2 if configured at grazing exodus, but the GZP diffraction angle can be normalized to maximize efficiency without sacrificing aperture, because a GZP does not rely on a secondary parabolic mirror at grazing exodus to focus starlight onto its spectrograph. The diffraction angle is determined by focal length which, in turn, determines the location and length of the secondary spectrograph receiver.

Our theoretical model for GZP efficiency is preliminary, but in the simplifying case of a fixed pitch volume holographic grating with sinusoidal fringes, equations published by Kogelnik [12] predict high efficiency at specific wavelengths at the Bragg angles that favor throughput. A sample calculation based on the Kogelnik equations is shown in Figure 8. Diffraction efficiency η varies with the thickness of the emulsion t and the change refractive index Δn as well as the angle of incidence α and angle of diffraction β, as calculated in the case of Figure 8 near to the Bragg angle. Efficiency is lower at an angle of incidence that conforms to the telescope GZP as per diagram in Figure 7, since the incident starlight broadband wavefront will arrive as a plane

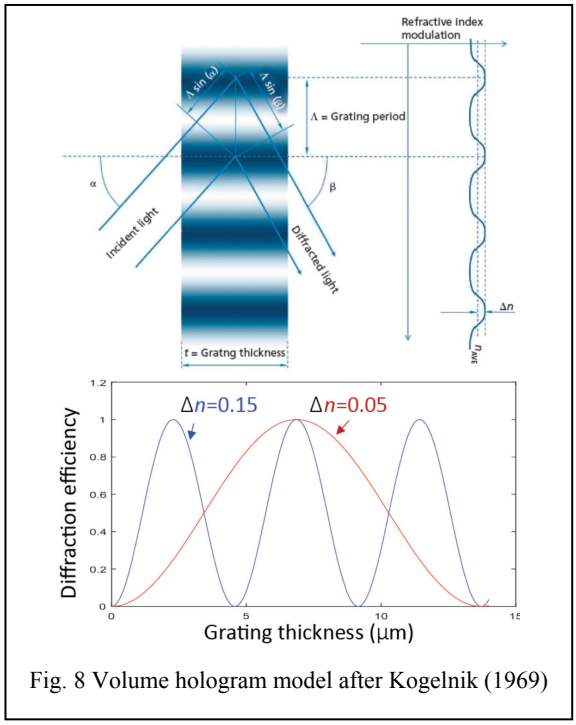

Fig. 8 Volume hologram model after Kogelnik (1969)

wave at α = 0°. We detail a method to more closely match angles α with β in Section 3.3, below. Even in the case where α = 0° in bench tests conducted by present co-author Dr. Mei-Li Hsieh, we recorded efficiencies of ~ 25% for a 16 μm thick polymer holographic film fabricated as a GZP demonstrating a telescope application. These results from the laboratory experiments are reported in detail in a separate conference session [13] and are sketched out within Section 3.2.

3.2 GZP Power

An analog holographic GZP inherits its focal lengths from the optics that make it. In the simple case of a paraxial recording, the thin lens focus equation $1/f = 1/f_o + 1/f_r$ (where f_o and f_r are the object and reference beam focal lengths) applies at the recording wavelength. Playback focal lengths otherwise vary inversely with playback wavelength. The point of focus f for playback wavelength λ_2 can be known for a GZP made with wavelength λ_1 by the ratio of (λ_1 / λ_2) so

$$f = \frac{\lambda_1}{\lambda_2}\left(\frac{1}{f_o} - \frac{1}{f_r}\right)^{-1} \quad (1)$$

In a bench experiment where the recording wavelength was a 515 nm diode laser and the focal lengths of the object and reference beams were 62 cm and 25 cm respectively, shown in Figure 9. the resulting GZP focal lengths are plotted against the prediction of Equation (1) in Figure 10.

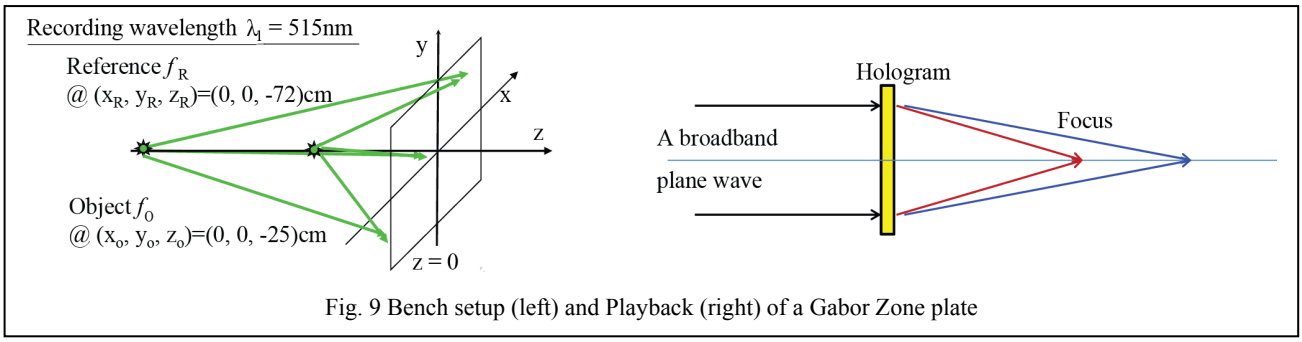

Fig. 9 Bench setup (left) and Playback (right) of a Gabor Zone plate

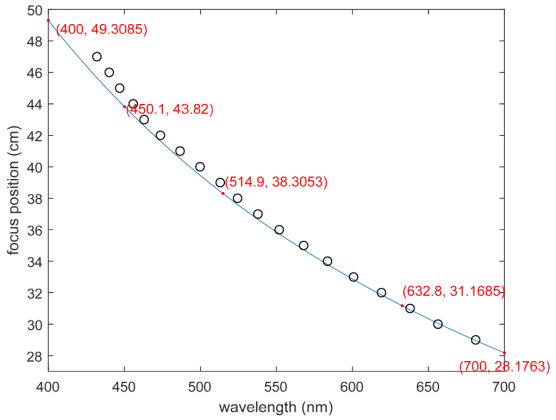

Fig. 10 Focal length vs. wavelength for a bench GZP

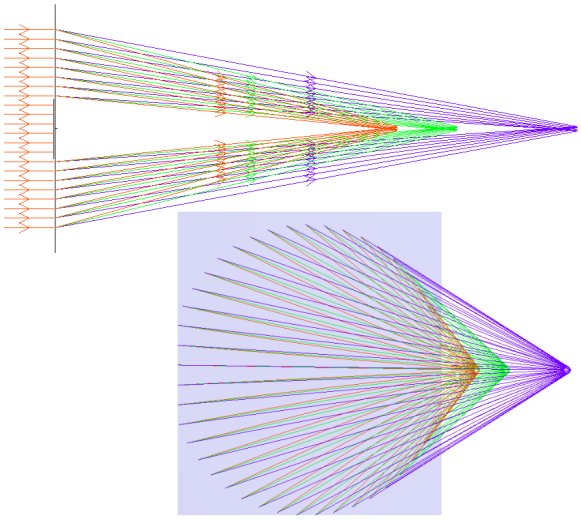

Fig. 11 Zemax model of GZP made with ring ray pattern: Orthogonal view (top) Rotated 30° off the normal (below)

The experiment simulated use of the GZP as a telescope primary objective where the incident source was a broadband plane wave in the visible regime. A Zemax model of the bench GZP is shown in Figure 11, using incident wavelengths of 400, 515, and 600 nm.. Although GZP's can be fabricated in reflection or transmission modes, in our models and experiments we are investigating transmission, because the specification for surface figure is far more relaxed in transmission than in reflection mode, especially when considering the intrinsic benefit of using a flat diffractive surface. If the GZP is printed on a thin pellicle surface, it will be tolerant of internal reflections. Given the anticipated deployment in negligible gravity, large gossamer membrane optics do not sag. Membrane support structures will be called for and are discussed in another section of this paper.

3.3 GZP modification for telescope application

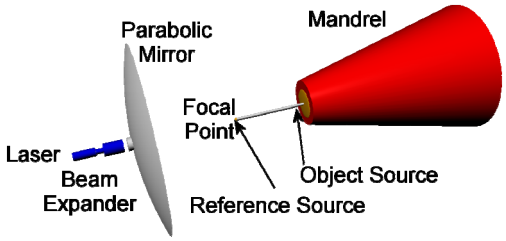

Fig. 12 Setup to record a hologram on a mandrel (red)

To form a central focal ring of considerable diameter as shown in Figure 7 rather than a line of focal points as shown in Figure 11, we consider a modification of conventional holographic recording so as to fabricate a three dimensional master in the form of a mandrel which is then used to emboss a flat annular surface. The strategy has benefits in that 1) the recording of the master can be realized with analog techniques without stitching error, 2) the embossed copy can be many times larger than the surface area of the mandrel, and 3) the geometric center of the resulting annulus can accommodate a secondary spectrometer. A drawing of the recording setup is shown in Figure 12. Laser illumination is reflected from two curved mirrors in front of the mandrel back toward a collimating mirror and then onto a sensitized surface on the mandrel. A Zemax model is shown in Figure 13.

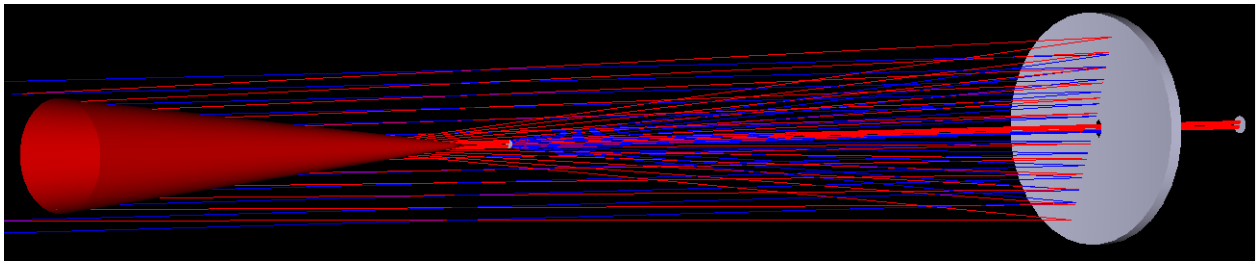

Fig. 13 Rays show one axis of a holographic recording. Reference beam (blue) is a plane wave. Object beam (red) converges.

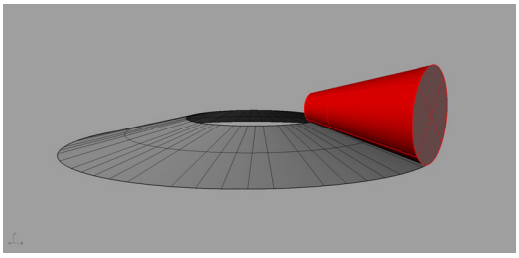

Fig. 14. Embossing on a truncated conical surface

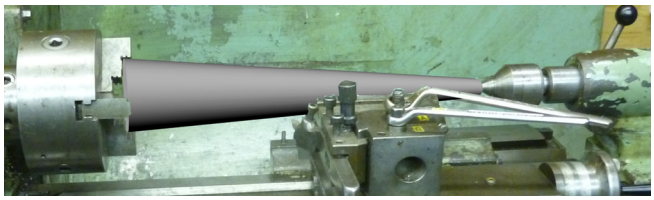

Fig. 15 Rendering of turning a metallic mandrel blank on rotary lathe

The mandrel geometry lends itself to embossing on a matched conical surface. When the GZP is printed at an incline as shown in Figure 14, the telescope will enjoy an incident angle $\alpha > 0°$, the condition required to maximize efficiency as per the math of Figure 8. The mandrel blank can be machined in metal on a lathe, Figure 15. The machined blank can subsequently be coated with holographic Shipley photo resist in a spin coater, Figure 16, and exposed by the reference and object beams as traced in Figure 13.

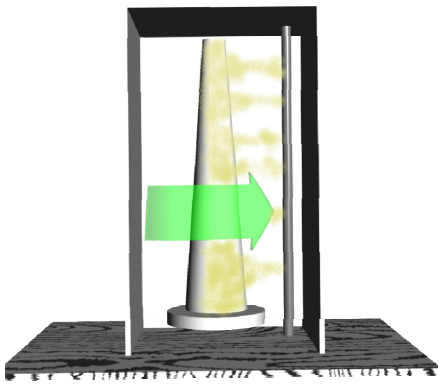

Fig. 16 Spin coating mandrel with photo resist
A sprayer bar applies the resist to a rapidly spinning mandrel in a vertical orientation.

Metallic optics made by diamond turning such as the blank for this holographically realized mandrel would appear to fall short of the surface figure expected of astronomical optics, but it has been a tenet of primary objective diffractive gratings that the constraints of mirrors and lenses do not apply to this novel approach, because performance is limited not by surface figure but by the uniform spacing between fringes or grooves that produce the interference pattern that resolves as discrete integer higher diffraction orders. Relaxed figure tolerance, particularly in the case of transmission primary objectives, became widely accepted as the FZP and photon sieve projects cited above received scrutiny over the past decade.

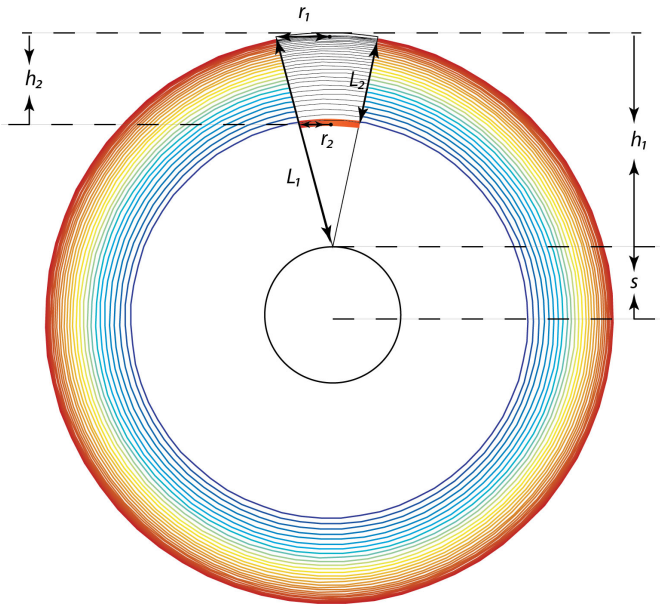

Fig. 17 Annulus (color) as embossed by GZP mandrel master

The area embossed by a holographic master in the form of a mandrel can be known by subtracting the inner clear disk from the area inscribed by the outer diameter. The area of the mandrel surface forming the GZP can be obtained by the equation for the area of the surface of a cone. Parameters are diagramed in Figure 17. The surface area of the annulus GZP is known from:

$$A_{\text{annulus}} = \pi\left((h_1 + s)^2 - (s + h_1 - h_2)^2\right) \quad (2)$$

The surface area on the mandrel required to produce the embossed impression is.

$$A_{\text{mandrel}} = A_1 - A_2 \quad (3)$$

where:

$$A_1 = \pi r_1 (r_1^2 + h_1^2)^{0.5} \quad (4)$$

$$A_2 = \pi r_2 (r_2^2 + (h_1 - h_2)^2)^{0.5} \quad (5)$$

dependencies which can also give L_1 and L_2, the lengths along the outside of the cone and mandrel, respectively. The focal length of the annulus is correlated to h_1. The radius s of Figure 17 is an added central void inside the annulus such that the GZP can focus on a cylindrical secondary, a spectrograph.

3.4 Secondary spectrograph

The wavefront collected by a GZP can be acquired in its first diffraction order with a spectrograph aligned with the wavelength dependent foci illustrated in Figures 9-11. An unambiguous spectrum can extracted beyond the free spectral range of the first-order if the spectrograph in the secondary is constructed from small diffracting facets each one of which facets filters a narrow wavelength band and passes that band into an optical fiber. The strategy is analogous to an échelle where a second disperser disambiguates overlapping higher-orders. Unlike an échelle, however, there is only the single higher-order, the second-order, which is incident at a distinctly different angle and at a different wavelength band that can be readily rejected at that specific wavelength if assigned to a specific facet with an appropriate holographic filter. A diagram of one holographic cell in the spectrograph is shown to the left hand side of Figure 18 with an example of its fabrication by analog holographic technique. A simplified schematic rendering of the spectrograph assembly is then shown on the right hand side of figure 18. If multiple wavelengths from two orders compete for injection into an optical fiber, only one is diffracted directly along the surface normal into a fiber tip while competitors from the second-order are diffracted away. The small size of the facets invites fabrication not only by classical analog holography, as illustrated, but also possibly by lithographic etching.

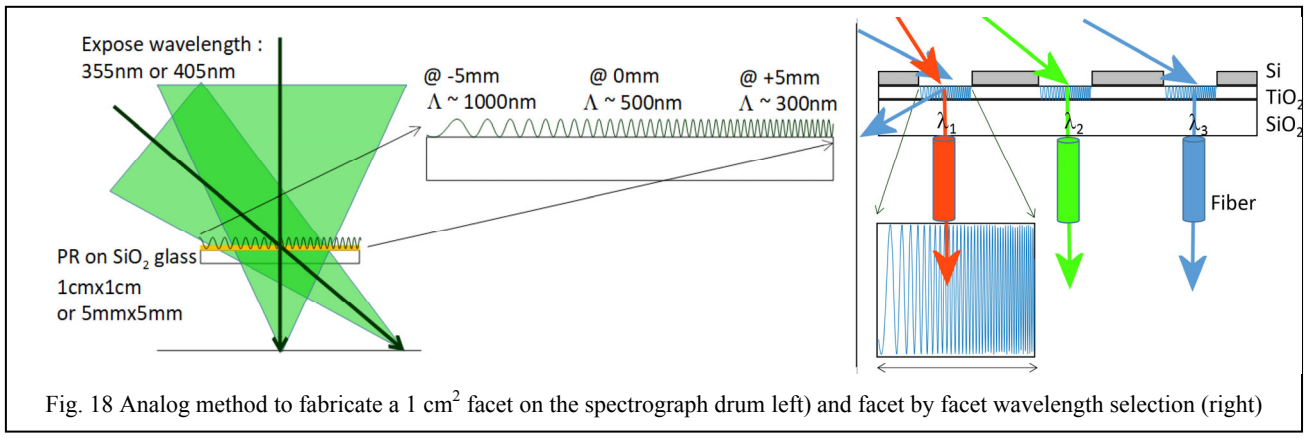

Fig. 18 Analog method to fabricate a 1 cm^2 facet on the spectrograph drum left) and facet by facet wavelength selection (right)

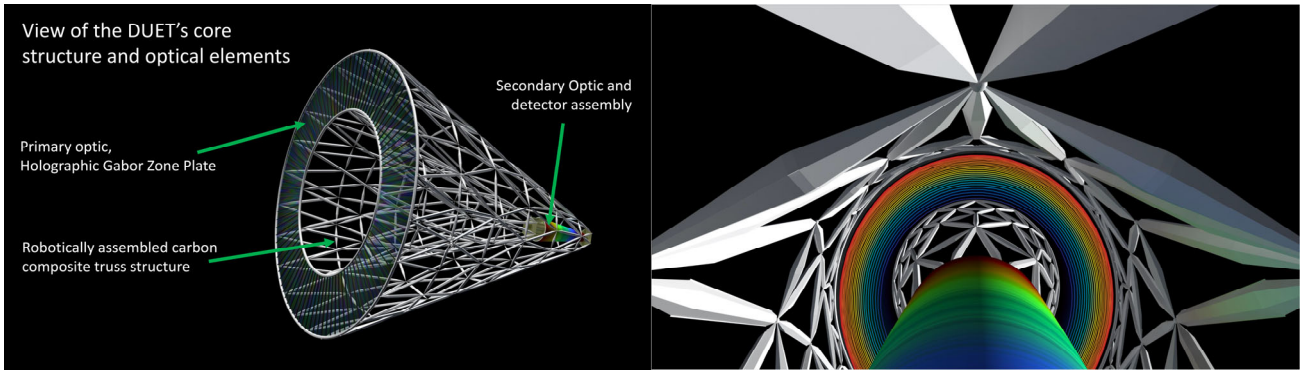

Fig. 19 Renderings of embodiment DUET with GZP and cylindrical spectrograph (left) view from spectrograph toward GZP (right)

A reduction to practice of the schematic of Figure 7, the Dual Use Exoplanet Telescope (DUET), is shown in a rendering of Figure 19 where the facets shown in Figure 18 are collectively wrapped onto a cylinder. The chromatically separated wavelengths are directed into the fibers schematically sketched in Figure 18. We use DUET here as a case study of the type of telescope without mirrors or lenses, in part, because it has unique features that address unresolved problems in space telescopes such as coronagraphy and areal mass.

3.5 Coronagraphy

Three novel types of coronagraphy are possible with a spectrographic telescope such as DUET.

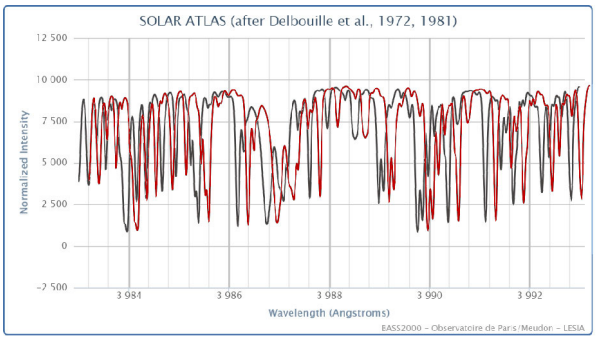

Fig. 20 Absorption line shift (after Delbouille *et al*)
Let red represent albedo phase against star's flux in black

First, it is possible to use the narrowly separated absorption lines of some stars, particularly G-class in the near U-V, to reduce flux ratios that without processing are typically 10^{10} to one between a star and its exoplanets. In Figure 20 the example of a Sun spectrum is used. A minimum in an emission line in the star may correspond in some cases to a peak in an exoplanet albedo. This is noticeable, for example, in the lines around 398.4 nm in the example given. This differential can approach three orders of magnitude, meaning that if measurements are taken at such bands, the contrast ratio may drop to 10^8:1 or better. If the absorption lines of the parent star are compared with the albedos of exoplanets around it, a translation of the reflected albedos spectra relative to the parent is caused by the slight change of angles incident upon the GZP coming from exoplanets.

A second coronagraphic method derives from Angular Differential Imaging, ADI.[14] If a star is perfectly centered in a preliminary image, it can be subtracted out if the image is rotated. Eccentric images rotate away from each other, so they do not null each other in the subtraction. As practiced in a GZP-based telescope, each resolved wavelength appears as a circle. These circles are significantly larger in radius than the image of the central star itself, Figure 21. The spectral circles spatially magnify the directly imaged star by 1000 times, facilitating the ADI process.

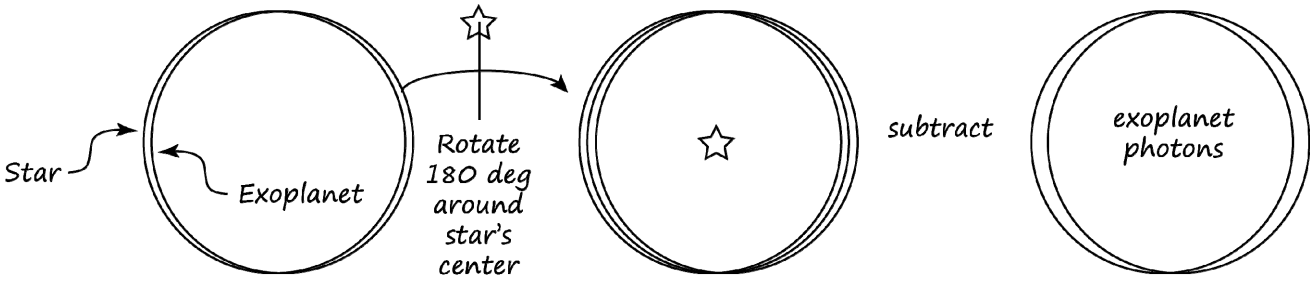

Fig. 21 ADI as practiced in DUET, shown here for a single extracted wavelength band.

A third coronagraphic method unique to a GZP dual dispersion architecture relies on the use of fiber fed spectral bands captured by the secondary spectrograph of Figure 18. Once a narrow wavelength band is transmitted by optical fiber, the trapped wave is compared interferometrically with the fiber associated with the same wavelength on the opposite side of the spectrograph. When the two fibers are mixed in a nulling interferometer, they can produce a central null at a common wavelength. Details of this spectrographic interferometer appear in a prior publication. [15] In brief, as is illustrated in Figures 22 and 23, fibers that subtend equal but opposite angles that illuminate a plane grating can be set to diffract into matched focusing mirrors (contrary to the title of this paper, mirrors do appear in this portion of the secondary) that are mixed to a common imaging plane where destructive interference occurs at a very narrow band, allowing slightly off-axis wavelengths from exoplanets to accumulate on the imager. The depth of the null is not yet known, but it is predicted down to four orders of magnitude by Zemax which produced the interferograms of Figure 24.

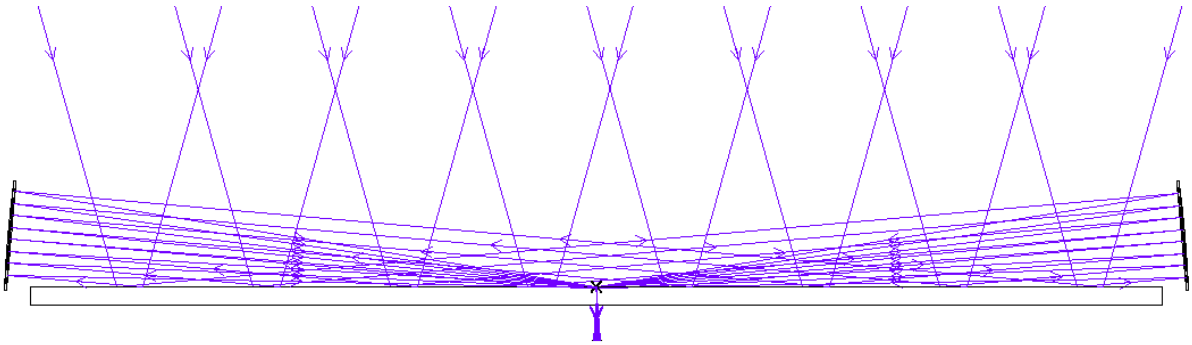

Fig. 22 Spectrographic nulling interferometer for star glare rejection
Central plane grating diffracts equal and opposite waves to focusing mirrors that mix to a common imaging plane

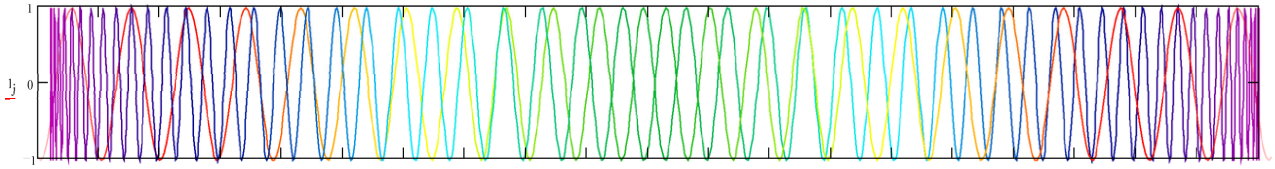

Fig. 23 Phase diagram of mixed equal and opposite wavelength bands where a null (green region) will occur in the center

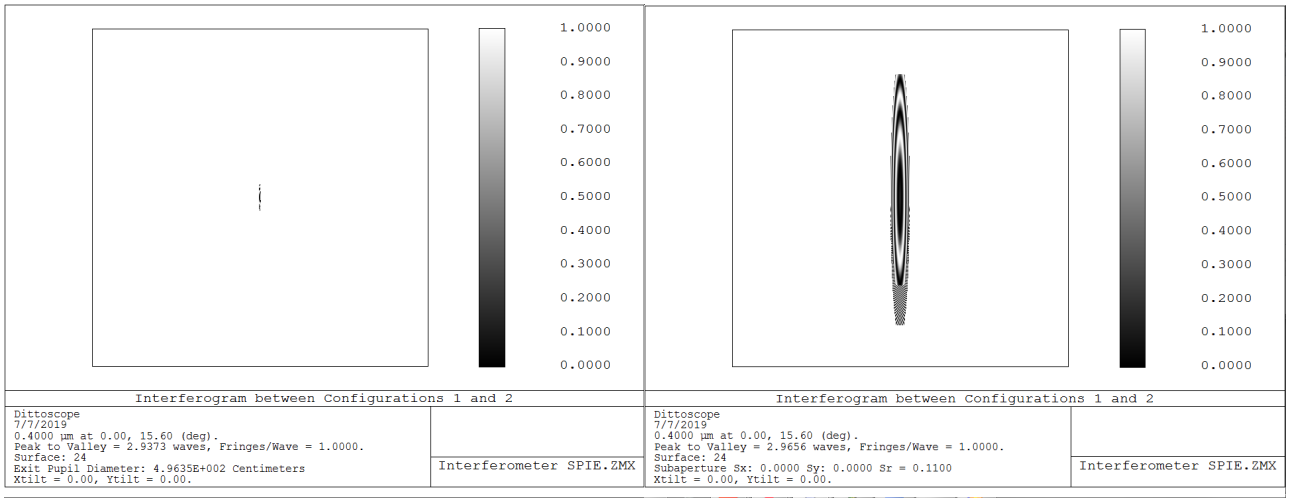

Fig. 24 Zemax interferogram of the nulling interferometer of Figure 22. Right side is a x 10 magnification of the image area

When fibers collect light from opposite sides of the annulus, the opposite sides can be phased. This implies that the angular resolution of the telescope is proportional to the outside diameter of the annulus. In models under study, while the ring could be 10 m from inner to outer diameter, the considerable diameter from one side of the annulus to the other may be in the 100 m range. Angular resolving power of diffraction primaries matches the fundamental diffraction limit of mirrors, that is to say, λ/D, meaning a 100 meter annulus could resolve into the milliarcsecond regime.

4. CONCEPT OF OPERATION

Mirror space telescope optics are conventionally prefabricated on the ground. JWST has been packaged in a compressed format for its launch sequence to be fully deployed later while in orbit. Because the larger the primary objective, the greater the resolution and collecting power, the need to engineer such compressed launch packages will be a continuing topic of investigation. The resulting challenges and tradeoffs recommend consideration of novel alternatives. Once in service, data acquired by space telescopes can be compressed to optimize transmission bandwidth. Lossless compression of image data is assumed. When the data is spectrographic in nature, new compression algorithms may be developed.

4.1 Stowage and on-orbit assembly

In the case of a gossamer membrane such as we propose, the GZP is packaged on a storage mandrel at launch and is unrolled in orbit. The geometry of the annular GZP is constrained in its narrow dimension by the vertical cavity under a launch vehicle fairing which can be upwards of 10 meters. The outside diameter of the deployed GZP is constrained by the support structure which poses mass limitation to transported trusses. To the extent that trusses can be stowed, the aperture can reach unprecedented dimensions. A preliminary study conducted by Tethers Unlimited of Seattle, WA (TUI) has a 50 to 100 meter aperture GZP telescope packaged for launch on a Space X heavy lift vehicle, Figure 25.

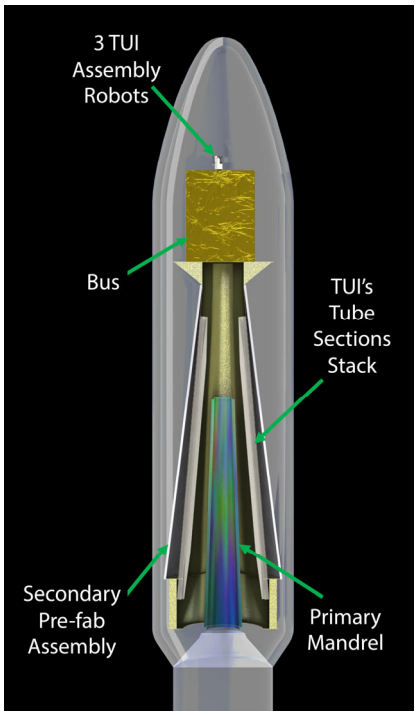

Fig. 25 Fairing section of Falcon Heavy

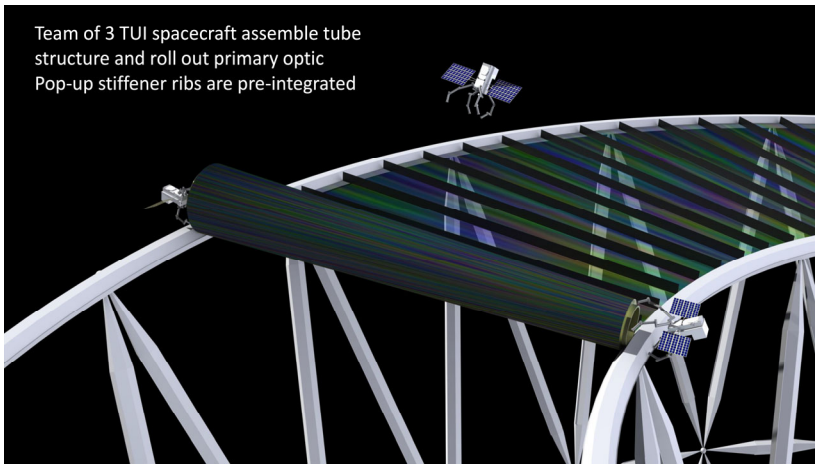

Fig. 26 TUI"Spider Bot" assembly of GZP primary objective onto trusswork

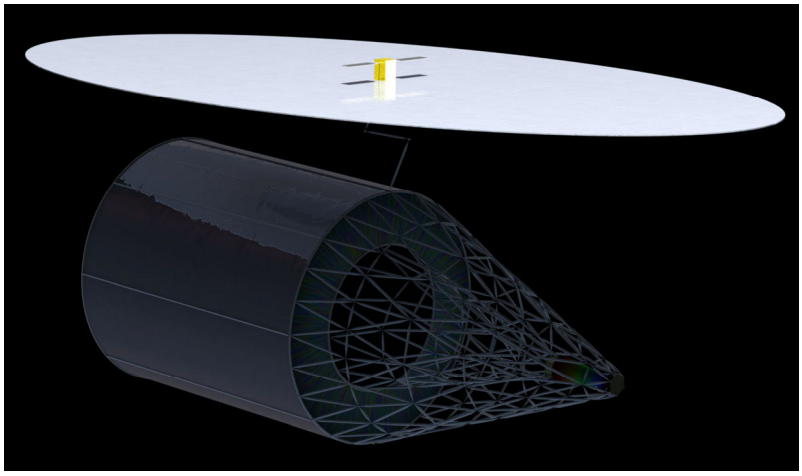

Fig. 27 DUET deployed behind sunshield

TUI has proposed two methods for creating trusswork. On the one hand, the trusses can be extruded from 3D printers. In this scenario, the raw material is delivered in tanks. Alternatively, trusses can be stowed as collapsed segments that open to form exoskeletal structures interlocking at vertices where hexapod positioners control dimensional posture and dampen vibrations. Both on-orbit methods rely on free flying robots that are seen unrolling the GZP from its mandrel storage in Figure 26. An artist rendering after deployment of the telescope is shown in Figure 27. The inlet tube faces the star, and the sunshield faces back to Earth from L-2.

4.2 Data reduction

The spectrogram of a GZP in the dual dispersion architecture consists of concentric circles, as shown in the diagram of Figure 21. In this example, the extraction of spectrographic data does not require that the telescope rotate, as is the plan for the Nancy Grace Roman space telescope. It uses software to disambiguate overlapping metamers through reorientation of entire physical instrument relative to proximate objects whose spectra intersect in any single image.[16] Double dispersion removes competing spectra by the mechanism illustrated in Figure 18 where a second-order blue is diffracted away from the fiber capturing a red band. Double dispersion was used in bench tests conducted with the laboratory experiment of Figure 28 where the behavior of a GZP was simulated with a circular plane grating. In this experiment a parent star could be simulated with a broadband incandescent source of blackbody radiation and exoplanet albedo was simulated with off-axis monochromatic lasers. Beams were combined with three pellicle beam splitters.

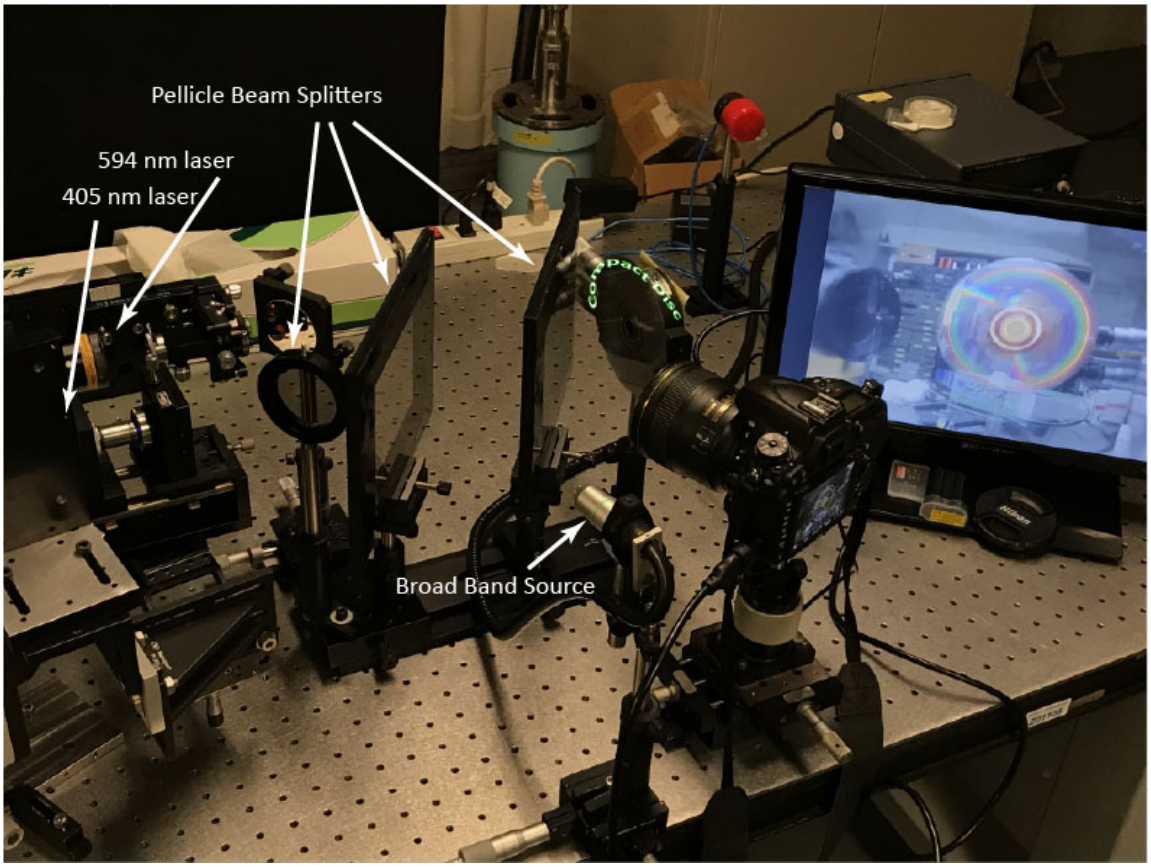

Fig. 28 Laboratory experiment to simulate behavior of GZP in an exoplanet spectrum acquisition campaign

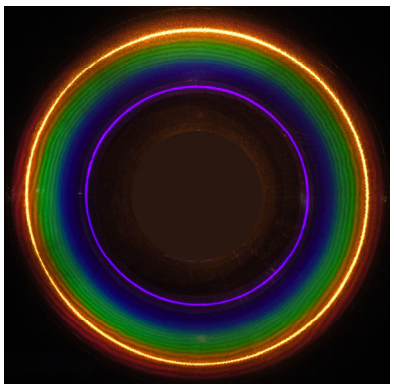

Fig. 29 Star & exoplanet

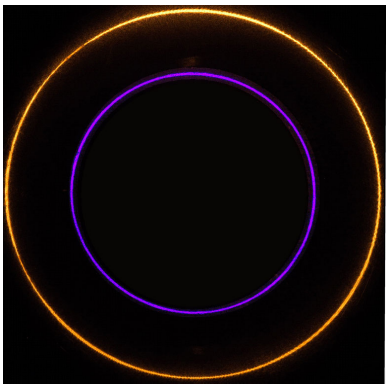

Fig. 30 Star violet & exoplanet yellow

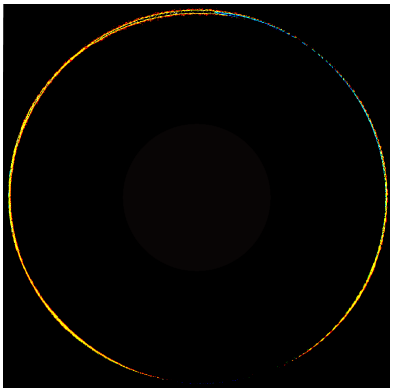

Fig. 31 Extracted exoplanet yellow

In the experiment of Figures 29-31, the spectra from all sources are shown in Figure 29. To simplify the experiment, the "star" source was extinguished except for its bright 405 nm violet band which is was subtracted leaving the off-axis "exoplanet" in its yellow band. In this example, there is a reduction of data to the presence of the 594 nm wavelength.

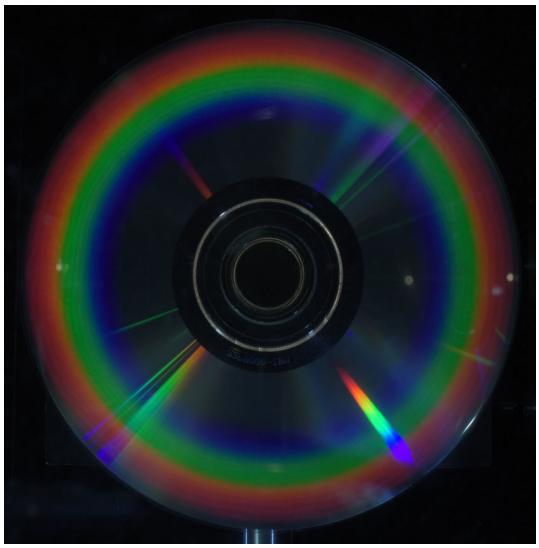

Fig. 32 On- and Off-axis focusing on a circular grating

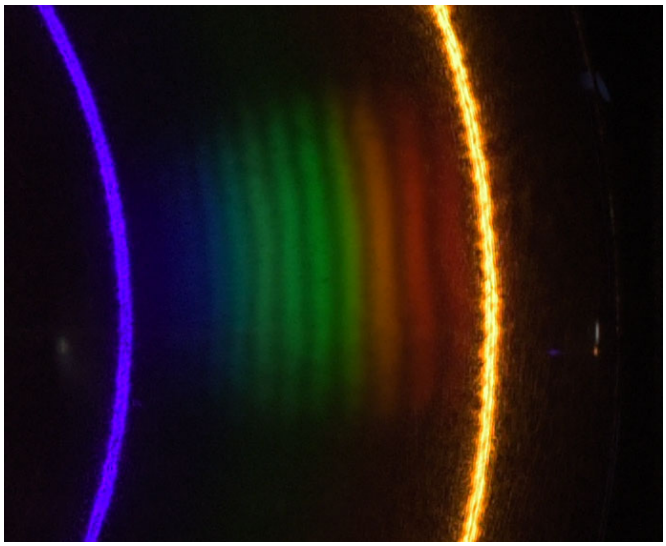

Fig. 33 Simulated broadband exoplanet spectrum

Spreading the limited photons of an exoplanet into a circular image 1000 times the diameter of its point source is prescription for photon starvation, however, it turns out that the off-axis light focuses into a relatively narrow spectral line. The phenomenon is exampled with a garden variety compact disc in Figures 32 and 33. While an on-axis source will generate a circle, an off-axis source concentrates light. On the bench of Figure 28, the broadband source was projected off-axis while the violet and yellow laser lines were aligned on the optical center. A detail of the resulting concentration of broadband light is shown in Figure 33 where the angle off-axis was several arc seconds.

In a campaign to survey for exoplanetary systems, the same GZP telescope can be used to detect radial velocity through Doppler shifts since the spectra from a star will expand or contract the diameter of the circle depending on whether the star is moving toward or away from us. A bench simulation of the effect is shown in Figure 34.

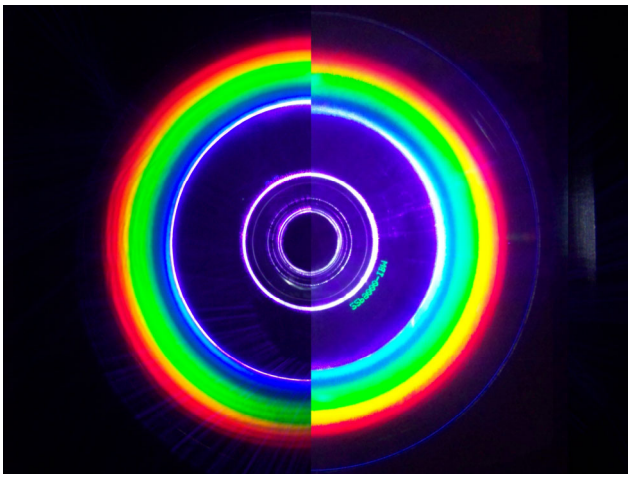

Fig 34 The diameter of a circular spectrogram records a simulation of the radial velocity of a star by Doppler shift.

5. CONCLUSION

A GZP can be thought of as a lens with severe chromatic aberration. By focusing its collected light onto a spectrographic secondary, the overlapping foci over the spectrum of wavelengths is disambiguated. The result could be an astronomical telescope without mirrors or lenses. The GZP is potentially a flat surface and can be supported on a gossamer membrane, reducing the complexity and areal mass of a space telescope. The output is intrinsically spectrographic which is a preferred data set for investigating the material substances and the motion of what are optically equivalent to point source objects. In an exoplanet astronomy campaign the telescope might return direct albedo spectra from exoplanets and indirect radial velocity Doppler shifts from stars. A hypothetical model telescope called DUET has been described.

Acknowledgements

This research was underwritten by the NASA Innovative Advanced Concepts program on grant 80NSSC19K0967. The authors are grateful to Professor Shawn-Yu Lin for his advice and access to his research laboratory at RPI.

REFERENCES:

[1] H. Philip Stahl *et al*, "Advanced ultraviolet, optical, and infrared mirror technology development for very large space telescopes," *J. Astron. Telesc. Instrum. Syst*. 6(2), 025001 (2020), https://doi.org/10.1117/1.JATIS.6.2.025001

[2] Isaac Newton, *Opticks*, (4th ed 1730), p. 46, http://www.gutenberg.org/files/33504/33504-h/33504-h.htm

[3] Thomas Ditto "The Dittoscope", *SPIE Proceedings*, 4840, Future Giant Telescopes, (30 January 2003); https://doi.org/10.1117/12.459878

[4] Thomas Ditto, "Kilometer scale primary objective telescope with no moving parts," *SPIE Proceedings* 4837, Large Ground-based Telescopes; (2003) https://doi.org/10.1117/12.458208

[5] Thomas D. Ditto, Kilometer scale telescope collector deployable in a Shuttle payload," *SPIE Proceedings* Volume 5578, Photonics North 2004: Photonic Applications in Astronomy, Biomedicine, Imaging, Materials Processing, and Education; (2004) https://doi.org/10.1117/12.606728

[6] http://www.3dewitt.com/telescope/slide1

[7] Ditto, Friedman and Baker, "Kilometer scale primary collector telescope," *SPIE Proceedings* 5578, Photonics North 2004; https://doi.org/10.1117/12.567574

[8] Thomas Ditto, "The Dittoscope," *op cit*, Figure 22

[9] Apai et al, "Nautilus Observatory: a space telescope array based on very large aperture ultralight diffractive optical elements," SPIE Proceedings, 11116, (2019) https://doi.org/10.1117/12.2529428

[10] James T. Early, Roderick Hyde, Richard L. Baron, "Twenty-meter space telescope based on diffractive Fresnel lens," Proc. SPIE 5166, UV/Optical/IR Space Telescopes: Innovative Technologies and Concepts, (30 January 2004); https://doi./10.1117/12.506232

[11] Geoff Andersen, "Large optical photon sieve," OPTICS LETTERS / Vol. 30, No. 22 / November 15, 2005

[12] Herwig Kogelnik, "Coupled Wave Theory for Thick Hologram Gratings," Bell System Technical Journal, 48: 9. November 1969 pp 2909-2947, https://archive.org/details/bstj48-9-2909

[13] Mei-Li Hsieh, Thomas D. Ditto, Shawn-Yu Lin, "Experimental demonstration of a Gabor zone-plate hologram for Space Exoplanet Telescope," *Advances in Optical and Mechanical Technologies for Telescopes and Instrumentation IV*, *Proc. SPIE*, 11451-192

[14] Christian Thalman, http://www.mpia.de/homes/thalmann/adi.htm

[15] Thomas D. Ditto "Self-nulling spectrograph for star glare rejection", *Proc. SPIE* 11117, Techniques and Instrumentation for Detection of Exoplanets IX, 111171P (9 September 2019); https://doi.org/10.1117/12.2525524

[16] M. Kummel *et al*, "The Slitless Spectroscopy Data Extraction Software aXe," *Astro. Soc. of the Pacific*, 121:59–72, 2009 January https://arxiv.org/abs/0812.1434